pHluo_M153R-CD63, a bright, versatile live cell reporter of exosome secretion and uptake, reveals pathfinding behavior of migrating cells

Bong Hwan Sung[1], Roxanne Pelletier[1] and Alissa M. Weaver[1, 2]

Departments of [1]Cell & Developmental Biology and [2]Pathology, Microbiology and Immunology, School of Medicine, Vanderbilt University, USA

Small extracellular vesicles (EVs) called exosomes affect a variety of autocrine and paracrine cellular phenotypes, including cellular migration, immune activation, and neuronal function. Understanding the function of exosomes in these processes requires a variety of tools, including live cell imaging. We previously constructed a live-cell reporter, pHluorin-CD63, that allowed dynamic subcellular monitoring of exosome secretion in migrating and spreading cells. However, there were some caveats to its use, including relatively low fluorescent expression in cells and the inability to make cell lines that stably express the protein. By incorporating a stabilizing mutation in the pHluorin moiety, M153R, pHluorin-CD63 now exhibits higher and stable expression in cells and superior monitoring of exosome secretion. Using this improved construct, we demonstrate visualization of exosome secretion in 3D culture and identify a role for exosomes in promoting leader-follower behavior in 2D and 3D collective migration. By incorporating a further non-pH-sensitive red fluorescent tag, this reporter allows visualization of the entire exosome lifecycle, including multivesicular body (MVB) trafficking, MVB fusion, exosome uptake and endosome acidification. This new reporter will be a useful tool for understanding both autocrine and paracrine roles of exosomes.

Introduction

Extracellular vesicles (EVs) are nano-sized vesicles secreted from cells with potent autocrine and paracrine biological activities[1]. Although EVs were first considered as cell debris with little biological relevance, EVs are now understood to constitute a fundamental mode of cell-cell communication that mediates delivery of specific protein, nucleic acid and lipid cargoes to recipient cells in diverse contexts[1, 2]. Indeed, EVs are involved in the pathogenesis of diverse diseases, including infections [3], neurodegenerative disorders[4], cardiovascular disease[5], and cancer[6, 7].

EVs can be classified by their size, biogenesis mechanism, cargoes, or density, e.g. small EVs, including exosomes, and larger EVs such as shed microvesicles (MVs) and large oncosomes[8]. Exosomes are a type of small EVs with diameter of 30 to 150 nm and have been the most studied with respect to their involvement in EV function[1, 2]. Exosomes are formed as intraluminal vesicles (ILVs) in late endosomal organelles called multivesicular bodies (MVBs) and secreted after fusion of MVBs with the plasma membrane. Several exosome biogenesis processes have been proposed, including capture of ubiquitinated cargoes by the endosomal sorting complex required for transport (ESCRT) machinery [9]. Syndecan-syntenin complexes also regulate exosome biogenesis via the ESCRT accessory protein Alix [10]. An ESCRT-independent biogenesis mechanism involving membrane curvature induced by ceramide generation by neutral sphingomyelinase 2 (nSMase2) has also been described[11]. Tetraspanin proteins such as CD9, CD63, and CD81 are frequently used markers of exosomes and other small EVs and may be involved in ILV cargo selection and/or biogenesis [12].

CD63 is a member of the tetraspanin superfamily, is enriched on ILVs in late endosomal MVBs, and is a broadly-used classic exosomal marker. Knockout expression of CD63 by CRISPR/Cas9 impairs secretion of small EVs but not LEVs, suggesting it contributes to exosome biogenesis [13]. CD63 has been used to label exosomes and track MVBs/exosomes in many studies[14-18]. However, most previous studies used pH-insensitive fluorescent proteins such as GFP or RFP, which led to extremely bright fluorescence of internal endosomes, limiting the ability to observe fusion events of MVBs with the plasma membrane due to a poor signal-to-noise ratio. To solve this problem, we adapted an approach from the synaptic vesicle field, that leveraged the properties of a pH-sensitive GFP derivative, called pHluorin, to observe dynamic vesicle fusion events [19]. pHluorin is virtually non-fluorescent under acidic conditions but fluoresces at neutral pH [19]. We first developed a pHluorin-tagged CD63 reporter to track exosome secretion and used it to demonstrate that MVB fusion precedes adhesion formation in spreading cells by 1-2 min [20]. We also observed that pHluorin-CD63-positive punctate trails were left behind migrating cells [20]. Subsequently, a similar reporter (pHluorin group placed 7 amino acids away from ours in the first extracellular loop of CD63) was used by the Pegtel group to study GPCR regulation of exosome secretion [21]. pHluorin-CD63 is a powerful tool to track exosome secretion and MVB fusion with the plasma membrane. However, while this construct is useful in 2-dimensional (2D) tissue culture conditions with high resolution imaging, the pHluorin moiety is subject to degradation in cells[22]. Thus, we are not able to stably express it in cells and its use for live imaging tends to be limited to select conditions by low and/or transient levels of expression and photobleaching.

In this study, we improved the stability and brightness of superecliptic pHluorin-CD63 by incorporating a single amino acid mutation, M153R, previously identified to stabilize ratiometric pHluorin in bacterial fusions [22]. We demonstrate that the mutated pHluorin-CD63, pHluo_M153R-CD63, can now be expressed as a stable construct in cells and is a bright reporter for exosome secretion. Using this construct, we are now able to resolve individual exosome puncta and observe pathfinding behavior of migrating cells along extracellularly deposited exosome trails in both 2D and 3D. By tagging an additional pH-insensitive red fluorescent protein to pHluo_M153R-CD63, we are further able to track multiple aspects of the exosome lifecycle, including MVB movements within cells before fusion, endocytosis of extracellular exosome deposits, and acidification of exosome-containing endocytic compartments.

Results

Mutation of pHluorin-CD63 creates a bright, stable live imaging reporter.

To improve on our previous reporter, we tested whether a mutation previously shown to stabilize ratiometric pHluorin in bacterial fusion proteins, M153R[22], would also stabilize our superecliptic pHluorin-CD63 construct. pHluorin-CD63 from our previous study[20] was mutated on Methionine 153 to Arginine by site-directed mutagenesis (pHluo_M153R-CD63, Fig. 1a). As shown in Fig 1b, CD63 is a tetraspanin protein with two extracellular loops. The pHluorin is inserted into the small extracellular loop at position 43. Upon fusion of MVB with the plasma membrane, the pHluorin moiety is exposed to neutral pH and becomes fluorescent which enables dynamic monitoring of exosome secretion (Fig. 1b). After site-directed mutagenesis, pHluo_M153R-CD63 was cloned into a lentiviral vector and stably expressed in HT1080 fibrosarcoma cells. To test whether pHluo_M153R-CD63 labels small EVs, conditioned media of pHluo_M153R-CD63-expressing HT1080 cells were collected and serially

centrifuged. Large EVs, typically containing shed microvesicles (MVs), were pelleted through a 10,000 x g spin for 30 min and small EVs, typically containing exosomes, were pelleted by centrifugation at 100,000 x g overnight. Nanoparticle tracking analysis (NTA) of small EVs showed the expected size distribution for exosomes with a peak diameter of 105 nm (Fig. 1c). Consistent with the previously reported role of pHluorin-CD63 as a reporter of MVB fusion and exosome secretion, immunoblotting of cell lysates and purified EVs revealed that pHluo_M153R-CD63 is exclusively detected in the exosome-enriched small EV preparation, and not in the larger MVs (Fig. 1d). Live cell imaging of HT1080 cells stably expressing pHluo_M153R-CD63 as well as the plasma membrane marker mCherry-CaaX revealed numerous pHluo_M153R-CD63-positive puncta left behind migrating HT1080 cells. These puncta were mCherry-CaaX-negative, suggesting that the deposition consists of exosomes and not plasma membrane-derived debris or MVs (Fig. 1e, Supplementary Mov. 1). These findings are similar to the previous green fluorescent "slime trails" that we observed left behind cells transiently transfected with pHluorin-CD63[20]; however, the deposited trails were much brighter and more easily resolved into puncta using standard epifluorescence imaging. Furthermore, the new reporter is able to be stably expressed in cells, which has many advantages, including capability of FACS sorting of populations for more uniform fluorescent expression, and imaging in more conditions, potentially including low light, lower resolution, 3D and *in vivo*.

Extracellular pHluo_M153R-CD63 puncta correspond to exosome deposits.

In a previous study, correlative light-transmission electron microscopy imaging revealed that fluorescent flashes of pHluorin-CD63 at the plasma membrane indeed correspond to MVB fusion events [21]. To determine whether pHluo_M153R-CD63 likewise reports exosome secretion, we knocked down the MVB docking protein Rab27a[23] with shRNA in pHluo_M153R-CD63-expressing HT1080 cells (Fig. 2a). As expected, the number of small EVs released into the media of Rab27a-KD cells was greatly decreased compared to control cells, as assessed by NTA (Fig. 2b). While not all small EVs are expected to be exosomes[24-26], a substantial portion of them are expected to derive from MVBs. Imaging of control and Rab27a-KD cells expressing pHluo_M153R-CD63 revealed greatly reduced extracellular deposition of pHluo_M153R-CD63-positive puncta by Rab27a-KD cells (Fig. 2c), as quantitated by measuring the area and integrated intensity of the pHluo_M153R-CD63-positive deposits surrounding the cells (Fig. 2d and e). pHluo_M153R-CD63-positive deposition also was observed from other cell types (Supplementary Fig. 1). Some of the puncta are brighter than others, suggesting that they may represent groups of exosomes. Furthermore, some puncta are arranged in linear trails, which may represent organization by cells as they migrate over them (e.g. as in Supplementary Mov. 1, trailing edge of migrating cell).

As further confirmation that the extracellular pHluo_M153R-CD63-positive puncta are exosomes, we colocalized them with other exosome markers (Fig. 2f). Immunostaining of fixed cells revealed that the ESCRT-I protein TSG101 was present in some extracellular pHluo_M153R-CD63 puncta. By contrast, immunostaining with the ESCRT accessory protein, Alix, revealed a near-perfect overlap with pHluo_M153R-CD63-positive extracellular puncta. This different localization pattern is consistent with the well-known heterogeneity of exosomes and with previous immunofractionation experiments in which an exosome biogenesis syndecan-syntenin-Alix complex accumulates in EVs immunoprecipitated with anti-CD63 antibody[10]. It could also be that TSG101 is less likely than Alix to be incorporated into exosomes during the biogenesis process, since there did not appear to be CD63-negative, TSG101-positive extracellular puncta. Of note, due to neutralization of intracellular pH by the paraformaldehyde

fixation procedure, pHluo_M153R-CD63 shows bright fluorescence in internal endosomal structures in these images (Fig. 2f).

To further determine whether pHluo_M153R-CD63 extracellular puncta and trails represent exosome deposition, we performed correlative light-electron microscopy (CLEM) in which HT1080 cells expressing pHluo_M153R-CD63 were first observed by epifluorescence microscopy followed by scanning electron microscopy (Fig. 2g). pHluo_M153R-CD63 fluorescence corresponded to small EVs with diameters ranging from 80 to 150 nm, which were frequently organized into linear trails (Fig 2g-i). By contrast, larger vesicles (e.g. the 774 nm EV in Fig 2g-i) were occasionally observed and were not fluorescent. These data are consistent with CD63 labeling primarily exosomes and not larger MVs[20, 27]. We also observed rare fluorescent pouches of small exosome-sized EVs left behind cells (Fig. 2g-ii). These pouches resemble previously described migrasomes[28], which are reportedly driven by a different tetraspanin, TSPAN4, or could alternatively represent groups of exosomes that derived from MVB fusion and tore off plasma membrane during cell migration. Additional mechanistic experiments would be required to identify their origin.

Cells exhibit pathfinding behavior over pHluo_M153R-CD63 deposits.

Previous reports indicate that exosome secretion promotes directional migration of several cell types including cancer cells[20, 29], neutrophils[30] and Dictyostelia[31]. To visualize dynamically how secreted exosomes influence cell migration, we performed live imaging under diverse conditions. In 2-dimensions, mCherry-CaaX/pHluo_M153R-CD63-double labeled HT1080 cells exhibited path-finding behavior along exosomes. Thus, cells extended leading edge protrusions toward and over exosome deposits labeled with pHluo_M153R-CD63 (Fig. 3a, arrows, Supplementary Mov. 2) and then migrated along the deposits (Fig. 3a, arrow heads). We observed the same phenotype in 3D collagen gels (Fig. 3c, Supplementary Mov. 3). To provide a quantitative assessment of this behavior, we analyzed the relationship of cell migration paths relative to exosomes by measuring the angle of each cell trajectory to the nearest exosome trail. We then took the cosine of the angle to obtain the pathfinding index. Thus, zero deviation of the path from an exosome trail is 1, i.e. if cells migrated directly toward the nearest exosome deposits or if cells migrated directly over the deposits. If cells migrated away from the nearest deposits in the opposite direction with a 180° angle, then the pathfinding index would be -1, as shown in the cartoons in Fig 3b and d. For both 2D and 3D migration, HT1080 cells primarily migrated toward or over exosome deposits with a median pathfinding index of 1 and 0.0607 and 0.0254 quartile ranges for 2D and 3D migration, respectively (Fig 3b and d).

Creation of a dual color reporter for MVB trafficking and fusion, and exosome uptake.

By imaging pHluorin-CD63, we previously observed by TIRF microscopy that putative MVB fusion events closely precede adhesion formation[20] in spreading cells. However, our ability to track and observe fusion events in other contexts was limited due to the dim fluorescence and lack of a pH-insensitive tag to track MVB trafficking events before fusion with the plasma membrane. To solve the latter problem, mScarlet, a bright monomeric red fluorescent protein[32] was cloned at the C-terminus of pHluo_M153R-CD63 to make pHluo_M153R-CD63-mScarlet. This construct exhibits only red fluorescence under acidic conditions (e.g. when contained in the MVB lumen) and both red and green fluorescence (making yellow) under neutral conditions (e.g. after secretion). Live confocal microscopy of HT1080 cells stably expressing pHluo_M153R-CD63-mScarlet showed that MVBs are frequently trafficked to protruding cell

edges and fuse there (Fig. 4a and Supplementary Mov. 4). Note the frequent appearance of CD63-mScarlet at the leading edge of migrating cells, often before membrane protrusion.

Both the trafficking of pHluo_M153R-CD63-mScarlet to the leading edge of migrating cells and the identified role of exosomes in directional migration [20, 30, 31] suggest that exosomes should be secreted from the front of migrating cells. However, it has been difficult under standard conditions to definitively determine whether exosomes are secreted at the front or back (or both) of migrating cells, especially since CD63 is both a plasma membrane protein and an exosomal protein. To more definitively answer this question, we placed pHluo_M153R-CD63-expressing HT1080 cells on a dish with a polymeric nanopatterned surface topography and performed confocal microscopy of moving cells (Fig. 4b. Supplementary Mov. 5). Due to the patterning of the substrate, new pHluo_M153R-CD63 deposits were easy to observe and track and revealed that exosome deposits largely stayed stationary as the cells moved over them. By defining < 2 μm of displacement length of the deposits as immotile, 85% of deposits are immotile suggesting that exosome deposits secreted under migrating cells stay stationary (Fig 4c and d). Furthermore, new exosome deposits (defined by violet color in heat map) clearly occurred at the front of the cell and were largely stationary as the cell moved over them, with reorganization of the deposits at the rear of the cell by retraction fibers.

It was previously shown by DIC and wide-field epifluorescence microscopy that exosomes can be captured by filopodia and endocytosed into cells[33]. Using the dual-color reporter, we observed a similar event in which migrating cells detect exosome deposits by touching them with filopodia, then migrate toward the exosome deposits and engulf them (Fig. 4e, white arrows, Supplementary Mov. 6). Although these experiments were not designed to identify mechanisms of endocytosis, in some cases we observed micropinocytosis-like uptake by engulfment (25 min frame, top arrow). Of note, endocytosed exosomes turned from yellow (pseudocolored white) to red (pseudocolored magenta) over time, consistent with maturation and acidification of endosomes (Fig. 4e, magenta arrows). From the time-lapse images, we quantified the kinetics of internalization and acidification of endocytosed exosome deposits. The internalization time of exosome deposits from the initial filopodial contact was highly variable and ranged from 1 min to 20 min with a median internalization time of 6 min (Fig. 4f). The distance between the exosome deposits and the plasma membrane likely affects the length of time taken for exosome uptake after initial contact. However, acidification of endocytosed exosome deposits, as visualized by loss of the pHluorin signal, occurred in a more narrow time range, from 2 to 11 min with a median of 7 min (Fig. 4g).

Discussion

Dynamic monitoring of EVs is critical to investigate roles of EV secretion in cell behaviors, especially cell-cell communication and cell migration. Although we previously developed a pH-sensitive exosome secretion reporter, pHluorin-CD63[20], the reporter was dim and could not be stably expressed in cells. By making a single amino acid mutation, we developed a stable and bright pH-sensitive reporter, pHluorin_M153R-CD63 for live imaging of MVB fusion, and cellular interactions with extracellular exosomes. Using this reporter, we observed that exosomes are secreted at the front of migrating cells and left behind in exosome trails. We also observed pathfinding behavior of migrating cells along trails of extracellular exosomes. Finally, we made a dual color reporter that allows observation of both exosome secretion and uptake by recipient cells.

Recently, there has been much interest in observing EV release and interchange between cells. GFP-CD63 and fluorophores tagged to palmitoylation motifs have been used to observe uptake by recipient cells within tumors[34]. In zebrafish, recent papers used both pHluorin-CD63 (injected as plasmid DNA) and a cyanine-based membrane probe to observe EV dynamics in the blood circulation [35, 36]. Our new reporters provide important additions to these tools by allowing stable expression in diverse cell types and potentially in transgenic animals while allowing high resolution imaging of subcellular events.

A key question addressed in this study is whether pHluo_M153R-CD63-positive extracellular puncta correspond to exosomes. As shown by Western blot analysis and CLEM, pHluo_M153R-CD63 labels small but not large EVs. In addition, KD of the MVB docking factor Rab27a[23] greatly reduced both the secretion of small EVs and the deposition of pHluo_M153R-CD63-positive extracellular puncta compared to control cells. Of note, there was a larger reduction in the area and intensity of extracellular CD63-positive deposits (Fig 2c-e) than in the number of secreted small EVs measured by NTA (Fig 2b). This discrepancy indicates the heterogeneity of small EVs and suggests the possibility of the release of small CD63-negative ectosomes from the plasma membrane, as has previously been described[26], as these would not be subject to regulation by Rab27a-mediated MVB docking. We also observed through immunofluorescent staining that pHluo_M153R-CD63-positive puncta are more highly overlapped with Alix, an ESCRT accessary protein, than with TSG101, an ESCRT-I protein. These data are consistent with a previous finding that syntenin regulates the budding of CD63-positive ILVs into MVBs by interaction with ALIX[10], although TSG101 was also involved in that process. One possibility is that TSG101 is less efficiently incorporated into the ILVs at the time of budding than Alix.

Exosome secretion promotes chemotaxis of several cell types[29-31]. Previously, we proposed a model in which exosomes secreted from cancer cells promote cancer cell chemotaxis in both an autocrine manner by secretion at the leading edge as well as in a paracrine manner by leaving behind exosome trails[29]. More recently, the Parent group reported that exosome trails released from migrating Dictyostelia induce streaming behavior [31]. In this study, we observed that cancer cells migrate toward and over exosome deposits to use them as migration tracks in 2D and 3D tissue culture environments. Although it is not clear how much of this behavior is due to chemicals released from the exosomes to induce chemotaxis and how much is providing an adhesive and signaling migration track, through direct interaction, the overall behavior is clear. Future studies using our reporter in conjunction with molecular manipulations should be able to dissect further these behaviors.

Another striking finding, observed with our dual color reporter, is that cancer cells migrate toward exosome deposits and actively endocytose them. Heusermann *et al*. reported that exosomes enter cells through filopodia a few years ago[33], a similar behavior to that of viruses[37]. However, for the first time, we visualized and quantitated both exosome uptake and the subsequent acidification of the endosomal compartments. We anticipate that future studies may be able to use this dual-color reporter to monitor exosome interchange between cells and whether endocytosed exosomes are recycled and re-secreted. Furthermore, by combining with inhibitors or molecular interventions, the dual reporter may be of use to study more precisely the endocytic fates of exosomes in diverse cell types.

Previous studies have reported that exosomes are likely secreted from the uropod or tail of migrating cells[38, 39]; however, those studies were performed with Dictyostelia and leukocytes which use amoeboid locomotion for the movement, involving the formation of posterior uropods. By contrast, directional sensing of cancer cells undergoing chemotaxis seems more likely to involve exosome

secretion at the leading edge of cells[29], at least for single cell autocrine migration events. Due to the fact that cells migrate over exosome paths, it has been difficult to discern where exosomes are secreted at a subcellular level. Using polymeric nanopatterned dishes, we observed clear deposition of pHluo_M153R-CD63-positive puncta at the front of migrating HT1080 cells. The deposited puncta stayed stationary as the cells moved over them and were then left behind migrating cells, with a small amount of reorganization. We also observed that migrating cells left bright retraction fibers at the trailing edge attached to the exosome deposits. The strong adherence of the cells to the secreted exosomes in both the nanopatterned substrate experiments and in our other movies is consistent with the adhesive function of exosomes that we previously observed in our studies[20, 29]. Due to the bright accumulation of previously deposited exosomes, we could not observe and cannot rule out additional deposition of exosomes at the rear of cells migrating on the nanopatterned plates; however, it is clear that exosomes are secreted at the cell front during migration.

To conclude, pHluo_M153R-CD63 is a stable and bright live cell reporter of exosome secretion. Migrating cells deposit pHluo_M153R-CD63-positive exosome trails behind them and the exosome trails attract and promote migration of follower cells. By tagging a pH-insensitive red fluorescent protein, mScarlet, to the C-terminus of pHluo_M153R-CD63, it was also possible to monitor MVB trafficking before fusion as well as exosome endocytosis. We anticipate that this reporter will be broadly useful to specifically investigate roles of exosome secretion and uptake in diverse physiological conditions.

Methods

Cell culture and reagents. HT1080 fibrosarcoma was maintained in DMEM supplemented with 10% bovine growth serum (BGS), MDA-MB-231 breast cancer cells and B16F1 mouse melanoma were maintained in DMEM supplemented with 10% fetal bovine serum (FBS) and HNSCC61 head and neck squamous cell carcinoma was maintained in DMEM supplemented with 20% FBS/hydrocortisone (0.4 μg ml^{-1}). A lentiviral shRNA expression system, pLKO.1, was used to knockdown Rab27a (TRCN0000005296 (5'-CCGG-CGGATCAGTTAAGTGAAGAAA-CTCGAG-TTTCTTCACTTAACTGATCCG-TTTTT-3') and TRCN0000005297 (5'-CCGG-GCTGCCAATGGGACAAACATA-CTCGAG-TATGTTTGTCCCATTGGCAGC-TTTTT-3'), ThermoFisher Scientific) or scrambled control (5'-CCTAAGGTTAAGTCGCCCTCG-3', Addgene Plasmid #26701). Viral particles were produced from 293FT cells by transfection of viral vectors. Cells were transduced by viral particles and selected using selection markers. For overexpression, low-expressing cells were sorted by FACSAria III (BD Biosciences) and used for experiments. HT1080 cells expressing both pHluo_M153R-CD63 and mCherry-CaaX were sorted for red fluorescence by FACSAria III after transducing mCherry-CAAX in HT1080-pHluo_M153R-CD63. Primary antibodies were: anti-CD63 (ab134045, abcam, 1:10,000 for WB), anti-GFP (A11122, Invitrogen, 1:1,000 for WB), anti-TSG101 (ab30871, abcam, 1:1,000 for WB and 1:100 for IF), anti-flotillin (610820, BD Biosciences, 1:1,000 for WB), anti-GM130 (610822, BD Biosciences, 1:250 for WB), anti-Rab27a (69295, Cell Signaling, 1:1,000 for WB), anti-Alix (2171, Cell Signaling, 1:200 for IF) and anti-β-actin (Ac-74, Sigma, 1:5,000). HRP- , or Alexa Fluor 546-secondary antibodies were from Santa Cruz Biotechnology or Invitrogen, respectively. Blots were imaged and analyzed using an Amersham Imager 600 (GE Healthcare Life Sciences).

Site-directed mutagenesis and cloning. Methionine153 on pHluorin in pcDNA3.1-pHluorin-CD63[20] was mutated to Arginine using QuickChange II XL Site-Directed Mutagenesis Kit (Agilent) with a pair of primers (Forward, 5'- ACG AGC ACT TGG TGT ACA TCC GGG CAG ACA AAC AAA AGA ATG-3' and Revers, 5'- CAT TCT TTT GTT TGT CTG CCC GGA TGT ACA CCA AGT GCT CGT-3'). pcDNA3.1-pHluorin_M153R-CD63 was subcloned into pENTR/D-TOPO and then cloned into pLenti6/V5-DEST plasmid using Gateway recombination cloning (ThermoFisher Scientific). mCherry-CaaX from pME-mCherry-CaaX (a generous gift from Chi-Bin Chien, University of Utah) was subcloned into into pENTR/D-TOPO and then cloned into pLenti6/V5-DEST plasmid using Gateway recombination cloning (ThermoFisher Scientific). mScarlet from pCytERM-mScarlet_N1 (a gift from Dorus Gadella, Addegene plasmid #85066) was cloned to the C-terminus of pHluo_M153R-CD63 in pLenti6/V5-DEST using Gibson Assembly Master Mix (NEB) with two pairs of primers (Forward, 5'- ACG AGC TGT ACA AGG GAT CCT AGA AGG GTG GGC GCG C-3' and Reverse, 5'-CCC TTG CTC ACC ATG AAT TCC ATC ACC TCG TAG CCA CTT CTG A-3' for pLenti6/V5-DEST-pHluo_M153R-CD63 and Forward, 5'- GAA GTG GCT ACG AGG TGA TGG AAT TCA TGG TGA GCA AGG GCG-3' and Reverse, 5'- TCG GCG CGC CCA CCC TTC TAG GAT CCC TTG TAC AGC TCG T-3' for pCytERM-mScarlet_N1). Site-directed mutagenesis and all subclonings were confirmed by sequencing (Genewiz).

Isolation of EVs. To collect conditioned media, 80% confluent cells were cultured for 48 h in Opti-MEM. Exosomes were isolated from conditioned media by serial centrifugation at 300 X g for 10 min, 2000 X g (4,000 rpm in Ti45 rotor) for 30 min, 10,000 x g for 30min (9300 rpm in Ti45), and 100,000 x g (30,000 rpm in Ti45) for overnight to respectively sediment live cells, dead cells, debris and large EVs, and small EVs. Pellets of large and small EVs were resuspended in PBS and spun again in same conditions. Each pellet was resuspended in PBS and used for NTA using ZetaView (Particle Metrix) or for Western blot analysis. At the time of conditioned media collection, cells were trypsinized and counted to allow for estimation of the exosome secretion rate as number of exosomes divided by the number of cells and by the number of hours of media collection.

Immunofluorescence staining. Cells on coverslips coated with FN (1 μg ml^{-1}) were permeabilized with 0.2% Triton X-100 in PBS after fixation with 4% paraformaldehyde in PBS. After blocking with 5% BSA in PBS, primary and secondary antibodies listed above were treated on the cells. After mounting coverslips on glass slides, Z-stack images were acquired with an LSM 510 laser scanning confocal microscope (CarlZeiss) equipped with a 63x/1.40 NA Plan Apo oil objective lens and processed by maximum intensity projection.

Correlative light-electron microscopy Cells were plated on high Grid-500 glass-bottom μ-Dishes (ibidi) coated with FN (1 μg ml^{-1}) and cultured at 37 °C incubator with 5% CO_2 for 1 day. Cells were initially washed in 0.1M sodium cacodylate buffer then briefly fixed in 2% paraformaldehyde. pHluo_M153R-CD63 overexpressing cells were identified using a Nikon Plan Apo 60x/1.40 oil immersion lens in a Nikon Eclipse TE2000E microscope equipped with a cooled charge-coupled device (CCD) camera (Hamamatsu ORCA-ER). The cells were then fixed in 2.5% glutaraldehyde in 0.1M cacodylate buffer, pH7.4 at room temperature (RT) 1 hour then transferred to 4ºC, overnight. The samples were again washed in 0.1M cacodylate buffer, then incubated 1 hour in 1% osmium tetraoxide at RT, rinsed in 0.1M cacodylate buffer. Subsequently, the samples were dehydrated through a graded ethanol series and then 3 exchanges of 100% ethanol and the glass-bottoms were taken off from the dishes, followed by critical point drying with the samdri-PVT-3D Tousimis critical point dryer. The dried coverslips were then

mounted on an aluminum stub with carbon adhesive tab and then sputter coated with gold using the Cresssington Sputter Coater 108. After coating for 60 seconds, the samples were imaged using a Quanta 250ESEM.

Live imaging. Cells were plated on glass-bottom MatTek dishes coated with fibronectin (1 μg ml^{-1}) and maintained in complete media at 37 °C incubator with 5% CO_2. At the next day, media was changed with Leibovitz's L-15 (Gibco)/10% serum or FluoroBrite DMEM (Gibco)/10% serum depending on CO_2 support to microscopes. Live imaging of mCherry-CaaX/pHluo_M153R-CD63-expressing HT1080 cells was performed with a Nikon Eclipse TE2000E microscope equipped with a 37 °C chamber and a cooled CCD camera. Images were captured using a Nikon Plan Fluor oil 40x/1.30 or Super Fluor 20x/0.75 NA objective lens. Still images of pHluo_M153R-CD63 were captured from diverse live cells using a Nikon Plan Fluor oil 40x/1.30. Time lapse movies of pHluo_M153R-CD63-expressing cells on nanopatterned glass-bottom dishes (800 nm width of both ridge and groove and 600 nm depth, Nanosurface Biomedical) coated with fibronectin (1 μg ml^{-1}), and for the dual reporter pHluo_M153R-CD63-mScarlet movies, were acquired with a Nikon A1Rconfocal microscope equipped with a Tokai Hit Incubation Chamber (37 °C with 5% CO_2) using Plan Apo 40x/1.3 NA oil immersion lens.

Kymograph analysis. Cells expressing pHluo_M153R-CD63-mScarlet were plated on glass-bottom MatTek dishes coated with fibronectin (1 μg ml^{-1}) and time lapse movies were acquired every 10 seconds with A1R-HD25 confocal microscope equipped with a Tokai Hit Incubation Chamber (37 °C with 5% CO_2) using Plan Apo 40x/1.3 NA oil immersion lens. Region of interest was selected by a rectangular selection tool and a time-series montage was made by using Fiji (Image/Stacks/Make Montage).

Quantitation of live imaging.

Quantitation of extracellular deposits: Cell bodies were carefully selected and deleted from each image. pHluo_M153R-CD63 deposits surrounding cells were segmented from the background by thresholding and measured for area and integrated intensity using Fiji (Analyze tab/Measure).

Pathfinding Index: Cell migration trajectorys were created using Fiji (Plugins/Tracking/Manual Tracking). Then, degree of angle (°) was measured between each trajectory and the closest exosome trails using the Angle Tool in Fiji. Degree was converted into radian (θ) and cosine value of radian was calculated using Excel, e.g. cos 0° = 1, cos 90° = 0, and cos 180° = -1. Only migratory single cells were selected for the analysis.

Nanopatterned substrates: To track and analyze mobility of pHluo_M153R-CD63 deposits on nanopatterned dishes, Imaris (Bitplane, vesicle tracking algorithm) and Fiji (Plugins/Mosaic/Particle Tracker 2D/3D) were used. It was defined that deposits with displacement length < 2 μm during one hour are immobile.

Numbers and Statistics. For both quantitated data and representative images from experiments, the n values and independent experiment numbers are listed in the figure legends. Quantitated imaging data were acquired from at least 3 independent experiments and multiple images or movies on multiple cells were captured. Cell numbers to be quantitated for each experiment were determined by our experience and data were excluded only if there is an obvious reason for poor data, such as dead or sick-looking cells. For non-quantitated Western blots (e.g. checking knockdown), they were generally

performed a single time. All datasets were tested for normality using the Kolmogorov-Smirnov normality test in GraphPad Prism. Non-parametric data groups were compared by the Mann-Whitney test and plotted as scatter plots with median and interquartile. Parametric data were compared using Student *t*-test and plotted as mean+/-standard error in scatter plots. The violin plot with median and interquartile range was created by Graphpad Prism to show all data.

References

1. Maas, S.L., Breakefield, X.O. & Weaver, A.M. Extracellular vesicles: unique intercellular delivery vehicles. *Trends in cell biology* **27**, 172-188 (2017).
2. van Niel, G., D'Angelo, G. & Raposo, G. Shedding light on the cell biology of extracellular vesicles. *Nature reviews Molecular cell biology* **19**, 213 (2018).
3. Schorey, J.S. & Harding, C.V. Extracellular vesicles and infectious diseases: new complexity to an old story. *The Journal of clinical investigation* **126**, 1181-1189 (2016).
4. Lee, J.Y. & Kim, H.-S. Extracellular Vesicles in Neurodegenerative Diseases: A Double-Edged Sword. *Tissue engineering and regenerative medicine* **14**, 667-678 (2017).
5. Dickhout, A. & Koenen, R.R. Extracellular Vesicles as Biomarkers in Cardiovascular Disease; Chances and Risks. *Frontiers in cardiovascular medicine* **5**, 113-113 (2018).
6. Xu, R. *et al.* Extracellular vesicles in cancer — implications for future improvements in cancer care. *Nature Reviews Clinical Oncology* **15**, 617-638 (2018).
7. Sato, S. & Weaver, A.M. Extracellular vesicles: important collaborators in cancer progression. *Essays in biochemistry* **62**, 149-163 (2018).
8. Zijlstra, A. & Di Vizio, D. Size matters in nanoscale communication. *Nature Cell Biology* **20**, 228-230 (2018).
9. Hurley, J.H. ESCRT complexes and the biogenesis of multivesicular bodies. *Current Opinion in Cell Biology* **20**, 4-11 (2008).
10. Baietti, M.F. *et al.* Syndecan–syntenin–ALIX regulates the biogenesis of exosomes. *Nature cell biology* **14**, 677 (2012).
11. Trajkovic, K. *et al.* Ceramide Triggers Budding of Exosome Vesicles into Multivesicular Endosomes. *Science* **319**, 1244-1247 (2008).
12. Andreu, Z. & Yáñez-Mó, M. Tetraspanins in extracellular vesicle formation and function. *Frontiers in immunology* **5**, 442-442 (2014).
13. Hurwitz, S.N., Conlon, M.M., Rider, M.A., Brownstein, N.C. & Meckes, D.G. Nanoparticle analysis sheds budding insights into genetic drivers of extracellular vesicle biogenesis. *Journal of Extracellular Vesicles* **5**, 31295 (2016).
14. Mittelbrunn, M. *et al.* Unidirectional transfer of microRNA-loaded exosomes from T cells to antigen-presenting cells. *Nature Communications* **2**, 282 (2011).
15. Koumangoye, R.B., Sakwe, A.M., Goodwin, J.S., Patel, T. & Ochieng, J. Detachment of Breast Tumor Cells Induces Rapid Secretion of Exosomes Which Subsequently Mediate Cellular Adhesion and Spreading. *PLOS ONE* **6**, e24234 (2011).
16. Corrigan, L. *et al.* BMP-regulated exosomes from Drosophila male reproductive glands reprogram female behavior. *The Journal of Cell Biology* **206**, 671-688 (2014).
17. Ventimiglia, L.N. *et al.* Cutting Edge: Regulation of Exosome Secretion by the Integral MAL Protein in T Cells. *The Journal of Immunology* **195**, 810-814 (2015).

18. Hurwitz, S.N. *et al.* CD63 Regulates Epstein-Barr Virus LMP1 Exosomal Packaging, Enhancement of Vesicle Production, and Noncanonical NF-κB Signaling. *Journal of Virology* **91**, e02251-02216 (2017).
19. Miesenböck, G., De Angelis, D.A. & Rothman, J.E. Visualizing secretion and synaptic transmission with pH-sensitive green fluorescent proteins. *Nature* **394**, 192 (1998).
20. Sung, B.H., Ketova, T., Hoshino, D., Zijlstra, A. & Weaver, A.M. Directional cell movement through tissues is controlled by exosome secretion. *Nature communications* **6**, 7164 (2015).
21. Verweij, F.J. *et al.* Quantifying exosome secretion from single cells reveals a modulatory role for GPCR signaling. *J Cell Biol*, jcb. 201703206 (2018).
22. Morimoto, Y.V., Kojima, S., Namba, K. & Minamino, T. M153R mutation in a pH-sensitive green fluorescent protein stabilizes its fusion proteins. *PLoS One* **6**, e19598 (2011).
23. Ostrowski, M. *et al.* Rab27a and Rab27b control different steps of the exosome secretion pathway. *Nature cell biology* **12**, 19 (2010).
24. Kowal, J. *et al.* Proteomic comparison defines novel markers to characterize heterogeneous populations of extracellular vesicle subtypes. *Proceedings of the National Academy of Sciences*, 201521230 (2016).
25. Thèry, C. *et al.* Minimal information for studies of extracellular vesicles 2018 (MISEV2018): a position statement of the International Society for Extracellular Vesicles and update of the MISEV2014 guidelines AU - Théry, Clotilde. *Journal of Extracellular Vesicles* **7**, 1535750 (2018).
26. Nabhan, J.F., Hu, R., Oh, R.S., Cohen, S.N. & Lu, Q. Formation and release of arrestin domain-containing protein 1-mediated microvesicles (ARMMs) at plasma membrane by recruitment of TSG101 protein. *Proceedings of the National Academy of Sciences* **109**, 4146-4151 (2012).
27. Van Niel, G. *et al.* The tetraspanin CD63 regulates ESCRT-independent and-dependent endosomal sorting during melanogenesis. *Developmental cell* **21**, 708-721 (2011).
28. Ma, L. *et al.* Discovery of the migrasome, an organelle mediating release of cytoplasmic contents during cell migration. *Cell research* **25**, 24-38 (2015).
29. Sung, B.H. & Weaver, A.M. Exosome secretion promotes chemotaxis of cancer cells. *Cell Adhesion & Migration* **11**, 187-195 (2017).
30. Majumdar, R., Tameh, A.T. & Parent, C.A. Exosomes mediate LTB4 release during neutrophil chemotaxis. *PLoS biology* **14**, e1002336 (2016).
31. Kriebel, P.W. *et al.* Extracellular vesicles direct migration by synthesizing and releasing chemotactic signals. *J Cell Biol*, jcb. 201710170 (2018).
32. Bindels, D.S. *et al.* mScarlet: a bright monomeric red fluorescent protein for cellular imaging. *Nature Methods* **14**, 53 (2016).
33. Heusermann, W. *et al.* Exosomes surf on filopodia to enter cells at endocytic hot spots, traffic within endosomes, and are targeted to the ER. *J Cell Biol* **213**, 173-184 (2016).
34. Lai, C.P. *et al.* Visualization and tracking of tumour extracellular vesicle delivery and RNA translation using multiplexed reporters. *Nature communications* **6**, 7029 (2015).
35. Hyenne, V. *et al.* Studying the fate of tumor extracellular vesicles at high spatiotemporal resolution using the zebrafish embryo. *Developmental Cell* (2019).
36. Verweij, F.J. *et al.* Live tracking of inter-organ communication by endogenous exosomes in vivo. *Developmental Cell* (2019).
37. Chang, K. *et al.* Filopodia and viruses: an analysis of membrane processes in entry mechanisms. *Frontiers in microbiology* **7**, 300 (2016).
38. Kriebel, P.W., Barr, V.A., Rericha, E.C., Zhang, G. & Parent, C.A. Collective cell migration requires vesicular trafficking for chemoattractant delivery at the trailing edge. *The Journal of cell biology* **183**, 949-961 (2008).

39. Shen, B., Fang, Y., Wu, N. & Gould, S.J. Biogenesis of the Posterior Pole Is Mediated by the Exosome/Microvesicle Protein-sorting Pathway. *Journal of Biological Chemistry* **286**, 44162-44176 (2011).

Acknowledgements

This study was funded by grants R01GM117916 and R01CA206458 to A.M. Weaver and 3U19CA179514-05S1 to R.J. Coffey, and supported by a voucher from Vanderbilt CTSA grant UL1 RR024975. The Vanderbilt Cell Imaging Shared Resources (CISR) is supported by a voucher from Vanderbilt CTSA grant FF_243306. We thank Ian McCara for use of his Nikon A1R confocal microscope and Matt Tyska, as well as members of the Weaver laboratory for extensive discussion. The content of this article is solely the responsibility of the authors and does not necessarily represent the official views of the National Institutes of Health.

Figure legends

Figure 1. pHluorin_M153R-CD63 is a bright, stable exosome reporter. (**a**) Sequence of pHluorin_M153R-CD63. pHluorin sequence is in green color. Highlighted regions in grey represent small (underlined) and large extracellular loops. M153R mutation is marked in red. (**b**) Diagram of pHluorin_M153R-CD63 construct. Notice pHluorin_M153R tag has bright fluorescence upon fusion of the multivesicular body (MVB) with the plasma membrane due to the exposure to neutral pH. Otherwise, it is non-fluorescent in the acidic condition of the MVB lumen. (**c**) Representative trace from nanoparticle tracking analysis of small EVs shows a typical exosome size profile. (**d**) WB with anti-GFP and anti-CD63 for cells and exosomes. Arrows indicate pHluorin_M153R-tagged CD63 while asterisk indicates cellular CD63. L, total cell lysate from parental cells. pL, total cell lysate from pHluorin_M153R-CD63-expressing cells. MV, microvesicles collected from conditioned media of pHluorin_M153R-CD63 cells. Exo, exosomes collected from conditioned media of pHLurin_M153R-CD63 cells. (**e**) Time lapse images from Supplementary Mov. 1 showing a migrating HT1080 cell stably expressing mCherry-CaaX (magenta) and pHluo_M153R-CD63 (green). Colocalization of magenta and green is white. Notice that the deposits left behind the migrating cell are only labeled with CD63 not with CaaX. Scale bar, 50 μm. Movie representative of 38 movies.

Figure 2. pHluorin_M153R-CD63-positive trails mark secreted exosomes. (**a**) Immunoblotting of Rab27a in pHluo_M153R-CD63-stably expressing HT1080. Sc, scrambled control. KD, knockdown. (**b**) Comparison of exosome secretion rate between control and Rab27a-KDs from 3 independent experiments. (**c-e**) Live imaging and analysis of extracellular pHluorin_M153R-CD63 between control and Rab27a-KD cells. (**c**) Representative images, n=31 from 3 independent experiments for each cell line. Scale bar, 30 μm. (**d**) Percentage of threshold area of the extracellular region from (**c**). (**e**) Integrated Intensity of the extracellular region from (**c**). (**f**) Immunofluorescence staining of fixed cells with exosomal markers, TSG101 and Alix (magenta). Arrows indicate colocalization of TSG101 (magenta) with pHluo_M153R-CD63-positive puncta (green) to form white. Note many white puncta in the CD63+Alix merged images. Scale bar, 30 μm. (**g**) Correlative light-electron microscopy of

pHluo_M153R-CD63-stably expressing HT1080. Zoom-in images from the left panel are shown at the right panel. *P<0.05; ***P<0.001.

Figure 3. Cells exhibit pathfinding behavior on exosome trails. (**a**) Time series images from live imaging of pHluorin_M153R-CD63 (with mCherry-CaaX) in 2D culture conditions (see Supplementary Mov. 2). mCherry-CaaX is shown in magenta and pHluorin_M153R-CD63 is shown in green in the merged image. n=186 cells from 31 movies from 4 independent experiments. Arrowheads indicate exosome trails. Arrows indicate protrusions. (**b**) Pathfinding index from (**a**) shown as a scatter-plot with median and quartile range. (**c**) Time series images from live imaging of pHluorin_M153R-CD63 (with mCherry-CaaX) in 3D collagen gels (see Supplementary Mov. 3). n=151 cells from 27 movies from 4 independent experiments. Arrowheads indicate exosome trails. Arrows indicate protrusions. Scale bars, 50 µm. (**d**) Pathfinding index from (**c**) shown as a scatter-plot with median and quartile range.

Figure 4. A dual reporter reveals MVB transport before fusion and endosome acidification after uptake. Live confocal microscopy was used to image pHluorin_M153R-CD63-mScarlet-expressing HT1080 cells. (**a**) Images were captured at 10 sec interval for 60 min (see Supplementary Mov. 4). Time-series images with 10 min interval show frames at the beginning and end of the movie, with the rectangle across the leading edge indicating location from which kymograph (middle) was derived. Kymograph shows events over time across the indicated rectangle. Two regions (i and ii) selected from kymograph (middle) are enlarged at the bottom. Magenta arrows in kymograph zoom indicate CD63-mScarlet trafficking and MVB docking to protrusions while white arrows indicate MVB fusion and exosome secretion. Scale bar, 50 µm. (**b**) Time series from Supplementary Mov. 5, showing trajectories of exosome deposits under the cell on a nanopatterned dish. Colors on heat map represent the time elapsed since deposition occurred. Note that violet color shows newly deposited exosomes. Note the image at the right bottom corner shows full tracks of exosome deposits. n=23 cells from 4 independent experiments. Scale bar, 50 µm. (**c**) and (**d**) Analysis of mobility of exosome deposits from movies as in (**b**) with scatter dot plots in (**c**) (mean +/- standard error) showing the percent of exosome deposits/cell with displacement length > or < 2 µm , where each dot represents the median displacement length of exosome deposits in that category from each single cell. ***P<0.001 (**d**) Total events (n=34052 from 23 cells) of displacement length are shown in a violin plot (median with interquartile range) from (**b**). (**e**) Time series images from live confocal microscopy of pHluorin_M153R-CD63-mScarlet-expressing HT1080 cells with 1 min interval from Supplementary Mov. 6. White arrows indicate examples where filopodia contact exosome deposits. Magenta arrows indicate acidified exosome-containing endosomal compartments after exosome uptake. n=45 exosome uptake events from 4 independent experiments. Scale bar, 25 µm. (**f**) Quantitation of internalization time of exosome deposits after initial filopodial contact from **e**. Median time from contact to uptake is marked by a dotted line. (**g**) Quantitation of time from exosome endocytosis to acidification as shown in (**e**). Median time of acidification is marked by a dotted line.

Figure 1.

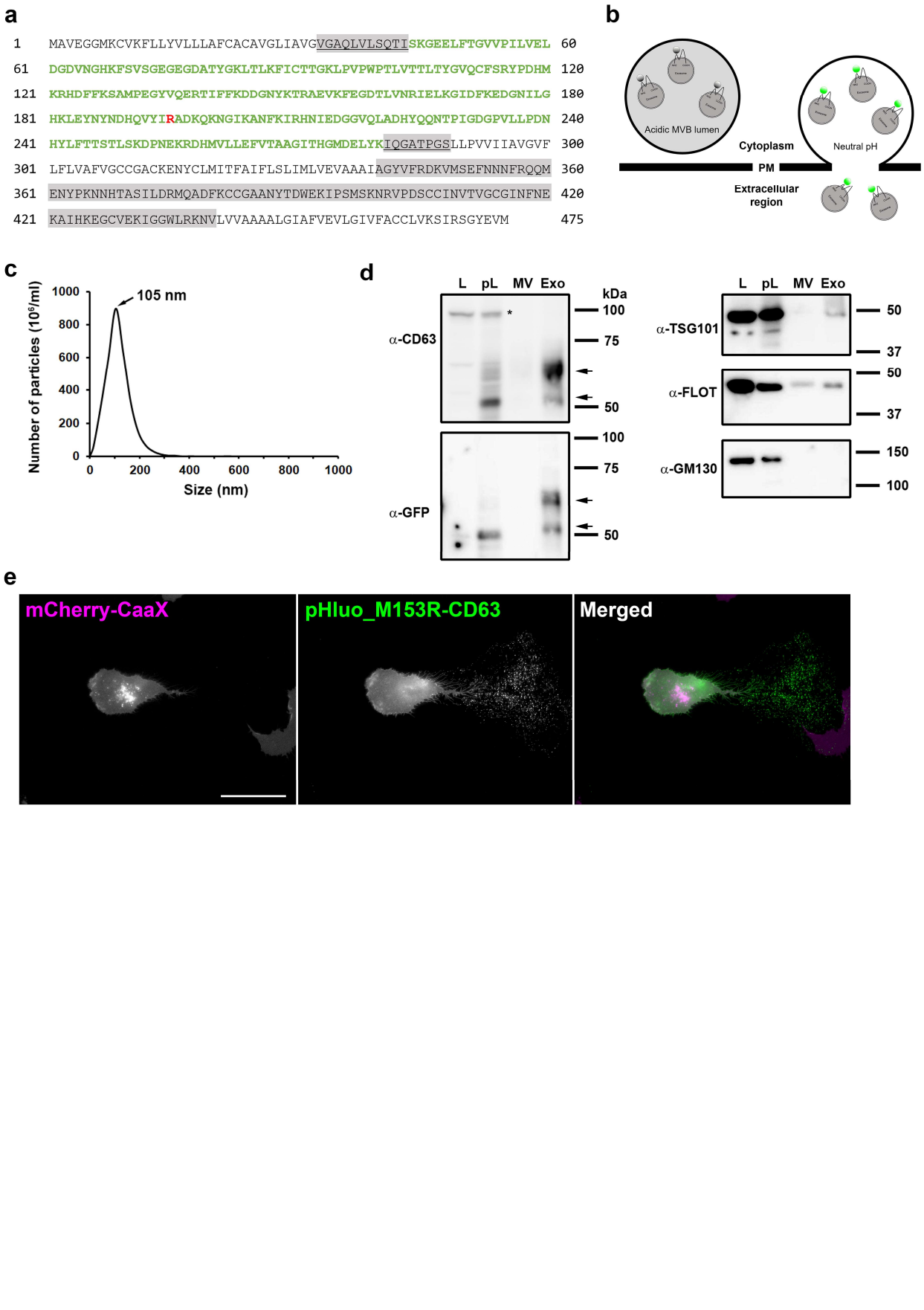

Figure 2.

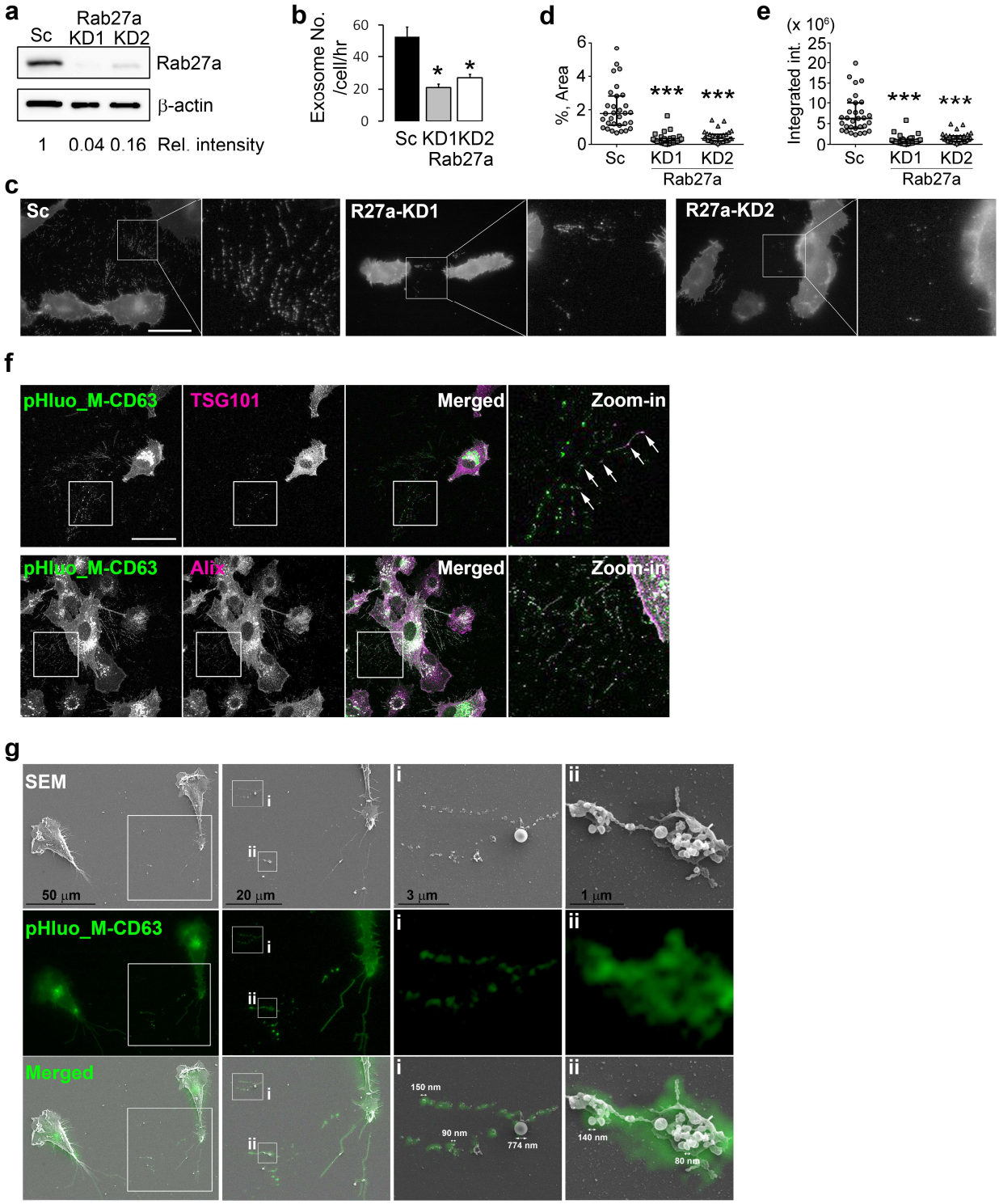

Figure 3.

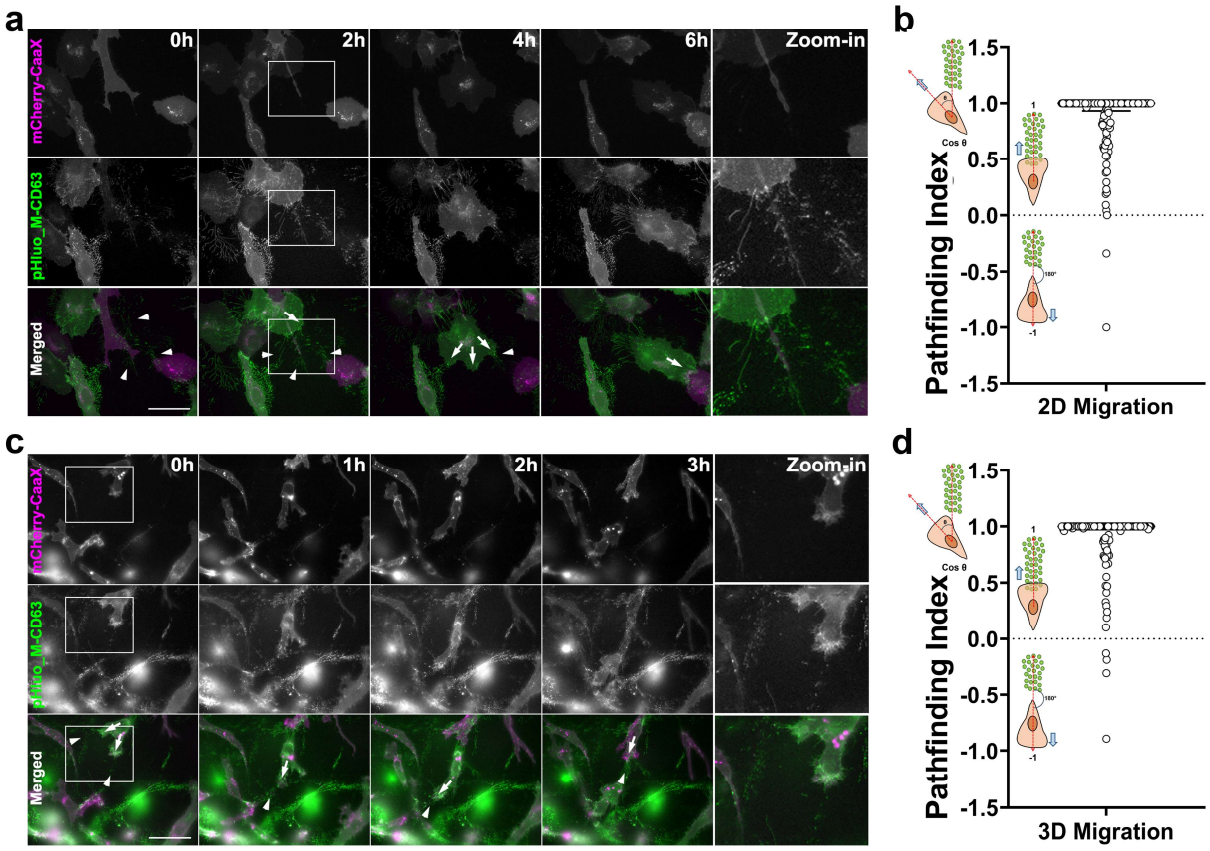

Figure 4.